Article:

ARTICLE

Tuning the hydroxyl functionality of block copolymer worm gels modulates their thermoresponsive behavior

Lucia Romero-Azogil,[a] Nicholas J. W. Penfold[b], * and Steven P. Armes[b], *

Over the past decade or so, polymerization-induced self-assembly (PISA) has become widely recognized as a powerful technology platform for the rational synthesis of sterically-stabilized diblock copolymer nano-objects in concentrated solution. In the present study, a binary mixture of water-soluble poly(glycerol monomethacrylate) ($PGMA_{59}$) and poly(ethylene glycol) (PEG_x, where x = 45 or 113) precursors were simultaneously chain-extended with 2-hydroxypropyl methacrylate (HPMA) using reversible addition-fragmentation chain transfer (RAFT) aqueous dispersion polymerization. For each of the two PEG blocks, a phase diagram was constructed at a fixed copolymer concentration of 10% w/w by systematically varying the target PHPMA DP (n) and the PEG mole fraction (z). The resulting diblock copolymer nano-objects are denoted using the general formula [z PEG_x + y $PGMA_{59}$]-$PHPMA_n$. Using a PEG block DP of 45 (i.e. x = 45), a pure worm phase was identified for just two diblock compositions when z = 0 (namely $PGMA_{59}$-$PHPMA_{150}$ and $PGMA_{59}$-$PHPMA_{160}$). In striking contrast, using a PEG block DP of 113 enabled twenty examples of pure worms to be obtained for z values ranging between 0.00 and 0.90. The thermoresponsive nature of these worms was assessed by tube inversion experiments and gel rheology studies. Importantly, reversible thermoresponsive behaviour was only observed when z ≤ 0.6 when targeting a PHPMA DP ≤ 180. Moreover, there was no evidence that inter-worm hydrogen bonding between the $PGMA_{59}$ and PEG_{113} stabilizer chains leads to stronger gels. These findings are expected to inform future studies focused on evaluating the minimum hydroxyl content of such worm gels that is required to induce stasis in embryonic human stem cells (see I. Canton et al., *ACS Central Science*, 2016, **2**, 64-75).

Introduction

Stimulus-responsive copolymers have been widely studied for both controlled drug delivery and tissue engineering,[1-10] which is an important research area within the field of regenerative medicine.[11-15] In particular, there are many literature examples of stimulus-responsive copolymer gels whose physical properties can be modulated by controlling the temperature, solution pH or exposure to light.[16-23]

In 2012 we reported the synthesis of thermoresponsive poly(glycerol monomethacrylate)-poly(2-hydroxypropyl methacrylate) (PGMA-PHPMA) diblock copolymer worms via RAFT aqueous dispersion polymerization of 2-hydroxypropyl methacrylate.[24] Such worms form soft, free-standing gels[25] in semi-concentrated aqueous solution at or above ambient temperature as a result of multiple inter-worm contacts.[26] Degelation occurs on cooling to 5 °C owing to a worm-to-sphere transition driven by surface plasticization of the PHPMA worm cores. Importantly, this morphological transition is reversible: worm reconstitution leads to gel reformation with essentially the same bulk modulus. Such thermoresponsive behavior enables facile sterilization of worm gels via cold ultrafiltration.[24] The excellent biocompatibility exhibited by these worm gels has enabled their use as a fully synthetic 3D matrix for long-term cell culture experiments.[27-29]

Interestingly, these worm gels share important physical properties with natural mucins: both systems are highly hydroxylated and exhibit relatively low bulk gel moduli (*G'* ~ 10–50 Pa).[42] Given that natural mucins are implicated in the induction of diapause (delayed gestation) with certain mammalian embryos,[30] we evaluated these worm gels as fully synthetic media for the long-term storage of naïve embryonic human stem cells.[7] Well-established protein assays confirmed that immersing such stem cell colonies into a PGMA-PHPMA worm gel induced stasis (i.e., a quiescent, non-proliferative state) that persisted for up to 14 days at 37 °C. On removal from the worm gel, the stem cells gradually returned to their former proliferative state over a 16 h period, with no apparent loss of pluripotency. Thus such worm gels may offer a potential cost-

a. *Departamento de Química Orgánica y Farmacéutica, Facultad de Farmacia, Universidad de Sevilla, 41012 Sevilla, Spain.*

b. *Department of Chemistry, Dainton Building, University of Sheffield, Brook Hill, Sheffield, South Yorkshire, S3 7HF, UK. Email: s.p.armes@sheffield.ac.uk; nick.penfold@syngenta.com*

effective storage medium to facilitate the global transportation of human stem cells from manufacturing facilities to point-of-use clinics and hospitals.[24, 25, 27, 31-34]

It is well-known that PEGylation can improve the pharmacological properties of certain proteins and drugs.[35-37] In the context of PISA, [23, 38-43] trithiocarbonate-capped PEG chains have been employed as a steric stabilizer block for various PISA formulations.[20, 44-47] However, unlike the *thermoreversible* behavior exhibited by PGMA-PHPMA worm gels, PEG$_{113}$-PHPMA$_{220}$ worm gels undergo an *irreversible* worm-to-sphere transition at 10% w/w solids on cooling from 25 °C to 4 °C.[44] This is because the relatively long PEG$_{113}$ chains confer effective steric stabilization on the spheres that are formed at 4 °C, which are thus unable to reform the original highly anisotropic worms via multiple 1D fusion events on returning to 25 °C. Instead, solely elastic collisions lead to kinetically-trapped spheres. In principle, this technical problem can be solved by utilizing a binary mixture of a PEG$_{113}$ and a PEG$_{45}$ for the RAFT aqueous dispersion polymerization of HPMA. Entropic mixing during PISA[48-52] ensures that all worms (and spheres) contain both long and short PEG chains, with the latter block modulating the efficacy of the steric stabilization mechanism. and thus facilitating worm reconstitution at ambient temperature via sphere-sphere fusion. Increasing the proportion of PEG$_{45}$ in the PISA formulation enabled the desired *thermoreversible* (de)gelation behavior to be achieved, albeit for a single diblock copolymer composition. Moreover, the bulk gel modulus at 37 °C could be readily adjusted simply by varying the copolymer concentration.[20] Informed by this initial study, we recently reported the rational design of new thermoreversible PEG$_{57}$-PHPMA$_n$ worm gels of comparable softness to PGMA-PHPMA worm gels to examine whether hydroxyl functionality plays a critical role in inducing stasis in pluripotent human stem cells.[27] Stem cell colonies continued to proliferate after immersion in such PEG$_{57}$-PHPMA$_n$ worm gels, with differentiation being observed if no adhesion substrate was present. Thus the *chemical functionality* of the hydrogel – rather than the bulk gel modulus - clearly plays a decisive role in the cell stasis induction mechanism.

Herein three water-soluble precursors (PGMA$_{59,}$ PEG$_{45}$ and PEG$_{113}$; see **Scheme 1**) are evaluated as steric stabilizer blocks for the synthesis of thermoresponsive diblock copolymer worm gels. Various binary mixtures comprising either PGMA$_{59}$ + PEG$_{45}$ or PGMA$_{59}$ + PEG$_{113}$ are used to prepare two series of diblock copolymer nano-objects *via* RAFT aqueous dispersion polymerization of HPMA, see **Scheme 2**. These series are denoted as [x PEG$_{45}$ + y PGMA$_{59}$] - PHPMA$_n$ and [z PEG$_{113}$ + y PGMA$_{59}$] - PHPMA$_n$ respectively. Prior to this study, it was not obvious to us that such PGMA/PEG combinations would be sufficiently compatible to be used for aqueous PISA formulations. This is because hydrogen bonding interactions were anticipated between the hydroxyl (H-donor) groups on the PGMA chains and the ether (H-acceptor) linkages on the PEG chains. On the other hand, if PGMA-water and PEG-water hydrogen bonding interactions dominate, then such binary compositions should be mutually compatible. In this latter (preferred) scenario, stronger worm gels could conceivably be

obtained owing to hydrogen bonding interactions between adjacent worms. If technically feasible, this dual steric stabilizer approach should enable the rational synthesis of thermoresponsive diblock copolymer worm gels for which the degree of hydroxyl functionality can be systematically varied. This is important because it should ultimately enable identification of the *minimum* hydroxyl content that is required to induce stasis in embryonic human stem cells.
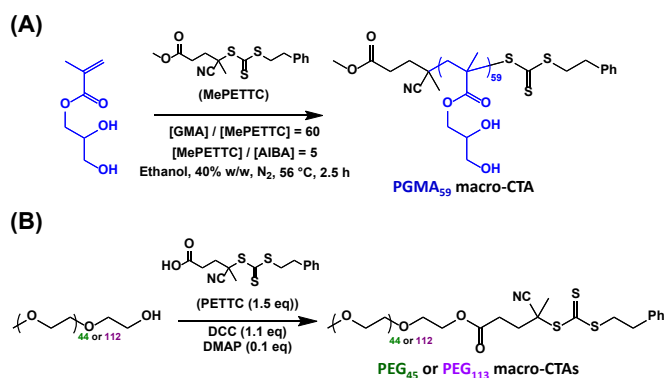
Scheme 1. (A) Synthesis of the PGMA$_{59}$ precursor used in this study *via* RAFT solution polymerization of GMA in ethanol at 40% w/w solids. (B) Synthesis of PEG$_{45}$ or PEG$_{113}$ precursors by Steglich esterification (mean degrees of esterification were calculated to be 94% and 95%, respectively). [Abbreviations: GMA = glycerol monomethacrylate; AIBA = 2,2'-azobis(2-methylpropionamidine) dihydrochloride; MePETTC = methyl 4-cyano-4-(2-phenylethanesulfanyl-thiocarbonyl)sulfanylpentanoate; PETTC = 4-cyano-4-(2-phenylethanesulfanylthiocarbonyl)- sulfanylpentanoic acid; DCC = *N,N'*-dicyclohexylcarbodiimide; DMAP = 4-dimethylaminopyridine].
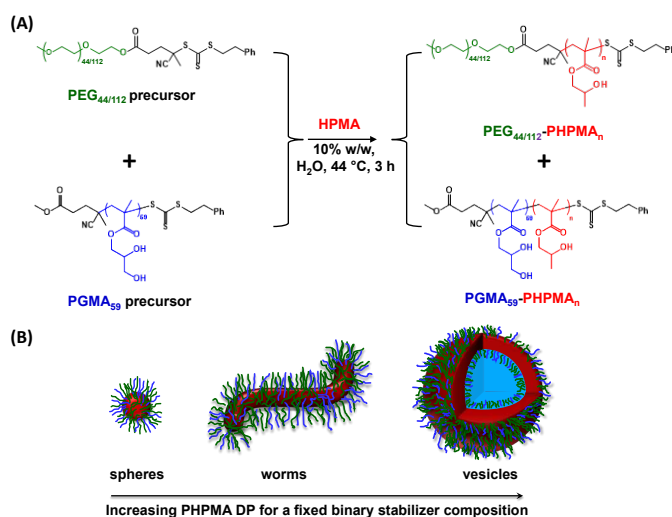
Scheme 2. (A) Reaction scheme for the synthesis of [x PEG$_{45}$ + y PGMA$_{59}$] - PHPMA$_n$ (**Route 1**) and [z PEG$_{113}$ + y PGMA$_{59}$] - PHPMA$_n$ (**Route 2**) diblock copolymer nano-objects *via* RAFT aqueous dispersion polymerization of HPMA at 50 °C. Here, *x, y, z* and n represent the mole fractions of PEG$_{45}$, PGMA$_{59}$, PEG$_{113}$ and the target PHPMA DP, respectively. **(B)** Schematic cartoon of the block copolymer morphologies that can be obtained with these PISA formulations. Note that the PEG$_{45/113}$ steric stabilizer chains are coloured green for both block lengths for clarity.

Experimental

Materials

N-N'-Dicyclohexylcarbodiimide (DCC; >99%), 4-dimethylaminopyridine (DMAP; >99%), 2,2'-azobis(2-methylpropionamidine) dihydrochloride (AIBA, >99%) poly(ethylene glycol) monomethyl ethers (PEG, M_n = 2,000 g mol^{-1}, mean DP = 45; M_n = 5,000 g mol^{-1}, mean DP of 113) were purchased from Sigma-Aldrich (UK). 2-Hydroxypropyl methacrylate (HPMA) was purchased from Alfa Aesar. Glycerol monomethacrylate (GMA) was kindly donated by GEO Specialty Chemicals Ltd. 2,2'-Azobis[2-(2-imidazolin-2-yl)propane] dihydrochloride (VA-044; >99%) was purchased from Wako Chemicals Ltd (Japan). Anhydrous dichloromethane was obtained from an in-house Grubbs purification solvent system. Deionized water (resistivity = 15 MΩ cm) was obtained from an Elgastat Option 3A water purification unit. All other chemicals or solvents (HPLC grade) were purchased from either VWR, Sigma-Aldrich or Fisher and were used as received.

Synthesis of the PETTC RAFT Agent

PETTC was synthesized according to a previously reported protocol.[53, 54] A 1 L conical flask was charged with a magnetic stirrer bar, sodium hydride (60% in oil, 7.0 g, 175 mmol) and diethyl ether (400 mL). 2-Phenylethanethiol (21.6 g, 156 mmol) was added dropwise to the stirred grey suspension, which turned white after 2 h. Carbon disulfide (13.5 g, 177 mmol) was added dropwise and a yellow precipitate of 2-phenylethanetrithiocarbonate was formed over 2 h. This product was isolated by vacuum filtration and dried overnight in a vacuum oven set at 30 °C. Solid iodine (23.0 g, 90.6 mmol) was added to a suspension of 2-phenylethanetrithiocarbonate (35.7 g, 151 mmol) in diethyl ether (400 mL). After stirring this suspension at 20 °C for 1.5 h, the resulting white precipitate of sodium iodide by-product was removed *via* filtration. The brown filtrate was washed with saturated sodium thiosulfate solution (4 x 150 mL), dried over magnesium sulfate and the solvent was removed under reduced pressure to afford bis-(2-phenylethanesulfanylthiocarbonyl)disulfide. A 1 L two-neck round-bottomed flask equipped with magnetic stirrer was charged with bis-(2-phenylethanesulfanylthiocarbonyl) disulphide (32.0 g, 75 mmol), ACVA (32.0 g, 114 mmol) and ethyl acetate (500 mL). This mixture was purged with nitrogen gas for 45 min then refluxed under nitrogen overnight. The resulting orange solution was washed with water (4 x 200 mL), dried over magnesium sulfate and all volatiles were removed under reduced pressure. The crude product was purified by column chromatography using silica gel as the stationary phase and a mobile phase comprising initially pure dichloromethane followed by a 95:5 v/v dichloromethane/ethanol mixed eluent after the first fraction had been removed to yield PETTC as an orange oil (72% yield). ^{1}H NMR (400 MHz, CD$_2$Cl$_2$, 25 °C): δ 1.91 (s, 3H, –(CN)C**H$_3$**), 2.40–2.62 (m, 2H, –(CH3)(CN)-C**H$_2$**CH$_2$COOH), 2.64-2.87 m, 2H, –(CH$_3$)(CN)-CH$_2$C**H$_2$**COOH), 3.02–3.06 (t, 2H, –PhC**H$_2$**CH$_2$S(C=S)S), 3.60–3.66 (t, 2H, –PhCH$_2$C**H$_2$**S(C=S)S), 7.25–7.40 (m, 5H, –**Ph**CH$_2$CH$_2$S(C=S)S). ^{13}C NMR (400 MHz, CDCl$_3$, 25

°C): δ 24.9 (**C**H$_3$), 29.5 (CH$_2$**C**H$_2$COOH), 33.5 (PhCH$_2$**C**H$_2$S), 34.0 (**C**H$_2$CH$_2$COOH), 38.0 (Ph**C**H$_2$CH$_2$S), 46.3 (S**C**(CH$_3$)(CN)CH$_2$), 118.9 (SC(CH$_3$)(**C**N)CH$_2$), 126.9-128.6, 139.2 (**Ph**CH$_2$), 177.1 (**C**=O), 216.4 (**C**=S). MS (ES$^+$) m/z calcd: 339.0 Found: 339.0 Anal. Calcd for C$_{15}$H$_{17}$NO$_2$S$_3$: C%, 53.07; H%, 5.05; N%, 4.13; S%, 28.33 Found: C%, 53.02; H%, 5.72; N%, 3.88; S%, 27.21.

Synthesis of the MePETTC RAFT agent

MePETTC was synthesized according to a previous protocol.[55] All glassware was dried in a 200 °C oven prior to use. A 250 mL round-bottomed flask was charged with PETTC (5.60 g, 16.5 mmol) and anhydrous dichloromethane (42 mL). The flask was immersed in an ice bath at 0 °C for 5 min. A separate 10 mL round-bottomed flask was charged with DMAP (450 mg, 3.7 mmol) and anhydrous methanol (3.54 mL, 8.74 mmol), then transferred to the PETTC solution *via* cannula under nitrogen. A third 10 mL round-bottomed flask was charged with DCC (3.60 g, 17.3 mmol) dissolved in anhydrous dichloromethane (10 mL) then transferred into the PETTC solution *via* cannula under nitrogen. This reaction mixture was stirred in the dark overnight at room temperature. The *N,N'*-dicyclohexylurea by-product was isolated via vacuum filtration and the crude product was purified by column chromatography (silica gel 60, dichloromethane eluent) and dried in a vacuum oven to isolate MePETTC as a viscous orange oil (3.97 g, 89% yield). ^{1}H NMR (400 MHz, CD$_2$Cl$_2$, 25 °C) δ 1.86 (s, 3H, -(CN)C**H$_3$**), 2.32–2.61 (m, 2H, -(CH$_3$)(CN)C**H$_2$**CH$_2$COOMe), 2.64–2.74 (t, 2H, -(CH$_3$)(CN)CH$_2$C**H$_2$**COOMe), 2.96–3.05 (t, 2H, -PhC**H$_2$**CH$_2$S(C=S)S), 3.56–3.63 (t, 2H, PhCH$_2$C**H$_2$**S(C=S)S), 3.68 (s, 3H, -COOC**H$_3$**), 7.20–7.36 (m, 5H, -**Ph**CH$_2$CH$_2$S(C=S)S). HRMS (ES$^+$) m/z calcd: 354.0651 Found: 354.0651. Anal. Calcd for C$_{16}$H$_{19}$NO$_2$S$_3$: C, 54.36; H, 5.42; N, 3.96; S, 27.21. Found: C, 53.92; H, 5.21; N, 3.34; S, 27.40.

Synthesis of the poly(ethylene glycol) (PEG$_{45}$ or PEG$_{113}$) precursors

All glassware was dried in a 200 °C oven for 24 h prior to use. A 1 L round-bottomed flask was charged with poly(ethylene oxide) monomethyl ether (M_n = 2000 g mol^{-1}, 40.4 g, 20.2 mmol) and toluene (800 mL). Toluene (~500 ml) was removed by distillation under nitrogen to remove residual water and the flask was cooled to 20 °C prior to addition of dichloromethane (~200 mL) to ensure full dissolution. A second 25 mL round-bottomed flask was charged with DCC (12.5 g, 60.6 mmol), DMAP (0.247 g, 2.02 mmol) and dichloromethane (10 mL) and this solution was then added to the PEG solution dropwise *via* cannula under a nitrogen atmosphere. A third 25 mL round-bottomed flask was charged with PETTC (10.28 g, 30.3 mmol) and dichloromethane (10 mL) and this solution was then slowly added to the PEG solution, which was stirred at 20 °C. After 16 h, the reaction solution was filtered and then concentrated under vacuum. Isolation was achieved *via* precipitation into cold diethyl ether (-78 °C; 2 L). This purification protocol was repeated twice more to isolate PEG$_{45}$-PETTC as a fine yellow powder, which was dried in a vacuum oven at 40 °C. End-group analysis by ^{1}H NMR spectroscopy indicated a mean degree of esterification of 94%. THF GPC

analysis indicated an M_n of 2,400 g mol^{-1} and an M_w/M_n of 1.04 relative to a series of PEG standards. Essentially the same protocol was used for the synthesis of the PEG$_{113}$ precursor. In this case, ^{1}H NMR spectroscopy indicated a mean degree of esterification of 95%. THF GPC analysis indicated an M_n of 5,800 g mol^{-1} and an M_w/M_n of 1.03 relative to PEG standards.

Synthesis of the PGMA$_{59}$ precursor by RAFT solution polymerization in ethanol

A 250 mL round-bottomed flask was charged with GMA (27.02 g, 168.9 mmol), MePETTC (1.00 g, 2.82 mmol), AIBN (92.8 mg, 0.57 mmol) and ethanol (42.01 g) to afford a 40% w/w orange solution ([GMA]/[MePETTC] = 60, [MePETTC]/[AIBN] = 5.0). The flask was sealed, placed in an ice/water bath and degassed under nitrogen for 30 min at 0 °C. This flask was placed in a preheated oil bath set at 70 °C for 2.5 h. The GMA polymerization was quenched by cooling to 20 °C with concomitant exposure to air. ^{1}H NMR spectroscopy analysis indicated 72% GMA conversion by comparing the integrated aromatic signals of the phenyl end-group at 7.4–7.8 ppm to the monomer vinyl signals at 6.2–6.4 ppm. Purification was achieved by precipitation into a twenty-fold excess of dichloromethane, with isolation of the crude product by vacuum filtration. This purification protocol was repeated twice more and the PGMA precursor was then dissolved in water, placed on a rotary evaporator to remove residual dichloromethane and freeze-dried for 48 h to afford a yellow powder. ^{1}H NMR analysis indicated a number-average degree of polymerization of 59 and no detectable residual GMA monomer. DMF GPC analysis indicated an M_n of 15,600 g mol^{-1} and a M_w/M_n of 1.15 (data expressed relative to a series of poly(methyl methacrylate) (PMMA) standards).

Synthesis of [x PEG$_{113}$ + y PGMA$_{59}$]–PHPMA$_n$ and [z PEG$_{113}$ + y PGMA$_{59}$]–PHPMA$_n$ diblock copolymer nanoparticles *via* RAFT aqueous dispersion polymerization of HPMA

A typical protocol for the synthesis of [0.40 PEG$_{113}$ + 0.60 PGMA$_{59}$]-PHPMA$_{160}$ diblock copolymers *via* RAFT aqueous dispersion polymerization of HPMA is as follows. A 14 mL sample vial was charged with HPMA (0.1872 g, 1.30 mmol), PEG$_{113}$ precursor (95% esterification, 0.0183 g, 3.26 µmol), PGMA$_{59}$ precursor (0.0476 g, 4.86 µmol), VA-044 initiator (0.52 mg, 1.61 µmol, (([PEG$_{113}$] + [PGMA$_{59}$]) / [VA-044] molar ratio = 5.0) and water (2.275 g) to afford a translucent yellow 10% w/w solution. The sample vial was sealed, cooled with the aid of an ice bath for 5 min, degassed with nitrogen for 30 min and then immersed in a preheated oil bath set at 44 °C for 3 h. The HPMA polymerization was quenched by exposure to air with concomitant cooling to 20 °C. ^{1}H NMR studies indicated more than 99% HPMA conversion. DMF GPC studies indicated an M_n of 32.8 kg mol^{-1} and a M_w/M_n of 1.19 (data expressed relative to a series of PMMA calibration standards). Two series of [m PEG$_{113}$ + g PGMA$_{59}$] – PHPMA$_y$ and [n PEG$_{45}$ + g PGMA$_{59}$]– PHPMA$_y$ diblock copolymers were prepared at 10% w/w solids by systematically varying the PGMA mole fraction (y) relative to that of either PEG$_{113}$ (z) or PEG$_{45}$ (x). Summaries of all the

diblock copolymer compositions, monomer conversions and molecular weight data for these syntheses are included in the supporting information (see Tables S1 and S2).

^{1}H NMR Spectroscopy

All ^{1}H NMR spectra were recorded using a 400 MHz Bruker Avance-400 spectrometer operating at 25 °C with 64 scans being averaged per spectrum. Spectra for PETTC, MePETTC, PEG$_{45}$ and PEG$_{113}$ were recorded in CD$_2$Cl$_2$. Spectra for PGMA$_{59}$ and each of the diblock copolymers were recorded in CD$_3$OD.

Transmission Electron Microscopy (TEM)

Aqueous block copolymer dispersions were diluted from 10% w/w to 2% w/w using deionized water and stirred overnight at 20 °C. These dispersions were then further diluted to 0.1% w/w and stirred for a further 3 h at 20 °C. Copper/palladium grids were surface-coated in-house to produce a thin film of amorphous carbon, which were then plasma glow-discharged for 30 seconds to afford a hydrophilic surface. A 10 µL droplet of the 0.1% w/w aqueous dispersion was placed on the hydrophilic carbon/palladium grid for 40 seconds, blotted to remove excess solution and then negatively stained using a 0.75% w/v aqueous uranyl formate solution (10 µL) for a further 20 seconds. Excess stain was removed by blotting with filter paper and the grid was carefully dried using a vacuum house. Imaging was performed using a FEI Tecnai Spirit 2 microscope operating at 80 kV and equipped with an Orius SC1000B camera.

Gel Permeation Chromatography (GPC)

Aqueous copolymer dispersions were freeze-dried overnight to obtain pale yellow powders. Dilute copolymer solutions (0.50% w/w) were then prepared in HPLC-grade DMF containing 10 mM LiBr with DMSO (1.0 % v/v) being used as a flow rate marker. GPC studies were conducted at 60 °C using DMF eluent at a flow rate of 1.0 mL min^{-1}. The GPC set-up comprised an Agilent 1260 Infinity series degasser and pump, an Agilent PL-gel guard column, two Agilent PL-gel Mixed-C columns and a refractive index detector. Sixteen near-monodisperse PMMA standards ranging from M_p = 645 g mol^{-1} to 2,480,000 g mol^{-1} were used for calibration. For analysis of the PEG$_{45}$ and PEG$_{113}$ precursors, GPC analysis employing THF eluent was used. This GPC set-up comprised an Agilent 1260 Infinity series degasser and pump, two Agilent PLgel 5 µm MIXED-C columns in series, a variable wavelength UV detector operating at 298 nm and a refractive index detector. The eluent contained triethylamine (2.0% w/w) and butylhydroxytoluene (0.05% w/v) and the flow rate was 1.0 mL min^{-1} at 30 °C. Either poly(ethylene glycol) standards with M_p values ranging from 238 g mol^{-1} to 86,200 g mol^{-1} or poly(methyl methacrylate) standards with M_p values ranging from 800 g mol^{-1} to 2,200,000 g mol^{-1} were used for column calibration.

Rheology

An AR-G2 rheometer equipped with a variable temperature Peltier plate and a 40 mm 2° aluminum cone was used for all rheology experiments. The storage modulus (G') and loss modulus (G'') were determined for 10% w/w aqueous copolymer dispersions as a function of temperature using an applied strain of 1.0 % and an angular frequency of 1.0 rad s^{-1}. Prior to rheology studies, worm gels prepared by **Route 2** were subjected to a thermal cycle, which consisted of cooling to 4 °C for 1 h followed by incubation at 25 °C for 24 h. Temperature sweeps were performed from 25 °C to 4 °C to 25 °C, with 5 min being allowed for thermal equilibration between each measurement.

Results & Discussion

Synthesis of the PGMA$_{59}$, PEG$_{45}$ and PEG$_{113}$ precursors

First, a PGMA$_{59}$ precursor was prepared using an trithiocarbonate ester-based RAFT agent (MePETTC)[17] *via* RAFT solution polymerization of GMA in ethanol (**see Scheme 1A**).

^{1}H NMR spectroscopy studies indicated a mean DP of 59 for the purified PGMA macro-CTA by comparing the integrated aromatic end-group signals at 7.2–7.4 ppm to that of the methacrylic backbone signals at 0–2.5 ppm (**Figure S1A**). DMF GPC analysis indicated a unimodal molecular weight distribution (**Figure S1B**), with M_n = 15.5 kg mol^{-1} and M_w/M_n = 1.14 being calculated relative to a series of near-monodisperse poly(methyl methacrylate) (PMMA) standards.

The PEG$_{45}$- and PEG$_{113}$-based RAFT agents were prepared from their monomethoxy precursors *via* Steglich esterification using an in-house synthesized carboxylic acid-functionalized trithiocarbonate-based RAFT agent known as PETTC[53, 56] (**Scheme 1B**). After purification, mean degrees of esterification of 94% and 95% were calculated for PEG$_{45}$ and PEG$_{113}$ respectively, by comparing the integrated oxyethylene protons assigned to PEG at 3.3-4.4 ppm to that of the aromatic end-group at 7.2-7.4 ppm (**Figures S2A** and **S3A**). DMF GPC analysis (expressed relative to PMMA standards) indicated an M_n of 4.4 kg mol^{-1} and an M_w/M_n of 1.04 for the PEG$_{45}$ precursor, while the PEG$_{113}$ precursor had an M_n of 8.7 kg mol^{-1} and an M_w/M_n of 1.09 (**Figures S2B** and **S3B**). Binary mixtures comprising the PGMA$_{59}$ precursor combined with either the PEG$_{45}$ precursor (**Route 1**) or the PEG$_{113}$ precursor (**Route 2**) were used to prepare two series of diblock copolymer nano-objects via RAFT aqueous dispersion polymerization at 50 °C (**Scheme 2**). These two series are hereby denoted as [x PEG$_{45}$ + y PGMA$_{59}$]-PHPMA$_n$ and [z PEG$_{113}$ + y PGMA$_{59}$]-PHPMA$_n$, where x, y and z represent the mole fractions of PEG$_{45}$, PEG$_{113}$ and PGMA$_{59}$, respectively and n is the target degree of polymerization (DP) for the hydrophobic PHPMA block. The experimental data obtained for **Routes 1** and **2** are discussed in turn below.

Route 1: Synthesis of [x PEG$_{45}$ + y PGMA$_{59}$] - PHPMA$_n$ diblock copolymer nano-objects

A series of [x PEG$_{45}$ + y PGMA$_{59}$] - PHPMA$_n$ diblock copolymer nano-objects was prepared by adjusting the PEG$_{45}$ and PGMA$_{59}$

mole fractions (x, y) while systematically varying the target PHPMA DP from 90 to 170. All such PISA formulations were conducted at 50 °C for 4 h targeting 10% w/w solids. **Table S1** summarizes the target diblock copolymer compositions, HPMA conversions, molecular weight data and copolymer morphology (assigned by TEM studies). More than 99% HPMA conversion was achieved in all syntheses, as determined by ^{1}H NMR spectroscopy studies. A typical ^{1}H NMR spectrum recorded for a [0.40 PEG$_{45}$ + 0.60 PGMA$_{59}$] - PHPMA$_{130}$ diblock copolymer redissolved in CD$_3$OD after freeze-drying the initial aqueous dispersion overnight is shown in **Figure 1**. The expected diblock composition was confirmed by comparing the integrated signals at 0.6–2.4 ppm for the common methacrylic backbone and pendent PHPMA methyl groups to the oxymethylene proton signals assigned to the PEG chains and the oxyethylene signals assigned to the GMA and HPMA repeat units at 3.5–4.2 ppm.

The molecular weight distribution of each block copolymer was assessed by DMF GPC using a series of near-monodisperse PMMA calibration standards. Given that the overall M_n is dominated by the PHPMA block, unimodal chromatograms were obtained for most block copolymer compositions (see **Figure 2**), with high blocking efficiencies being achieved for both the PGMA$_{59}$ and PEG$_{45}$ precursors. Increasing the target PHPMA DP produced higher M_n values for a fixed steric stabilizer composition (*i.e.* constant x), as expected. In addition, a reduction in M_n was observed when a higher PEG mole fraction was utilized as the stabilizer block (i.e. higher x) for a given target DP of the core-forming PHPMA block. This is simply

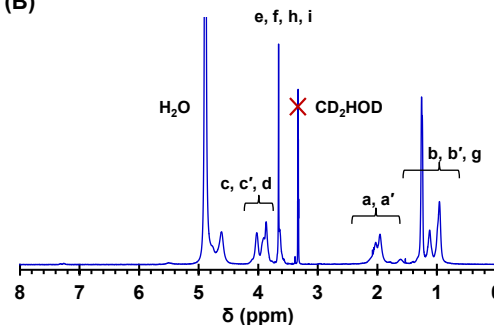**(A) [0.40 PEG$_{45}$ + 0.60 PGMA$_{59}$]-PHPMA$_{130}$**
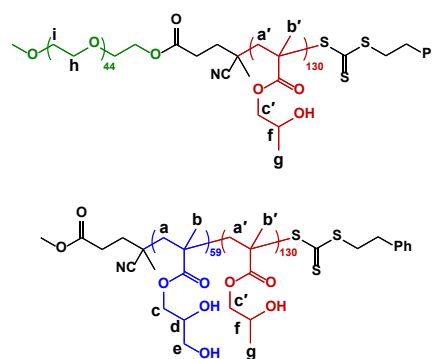
(B)

Figure 1. (A) Chemical structure and (B) partially assigned ^{1}H NMR spectrum recorded for [0.40 PEG$_{45}$ + 0.60 PGMA$_{59}$] - PHPMA$_{130}$ diblock copolymer redissolved in CD$_3$OD after freeze-drying the as-synthesized aqueous dispersion.

(A)

G$_{59}$H$_{170}$
M_n = 38.3 kg mol^{-1}
M_w / M_n = 1.17
G$_{59}$
M_n = 15.5 kg mol^{-1}
M_w / M_n = 1.14

(B)

[0.40 P$_{45}$ + 0.60 G$_{59}$]-H$_{170}$ G$_{59}$ P$_{45}$
M_n = 43.7 kg mol^{-1}
M_w / M_n = 1.20

(C)

P$_{45}$H$_{170}$
M_n = 27.1 kg mol^{-1}
M_w / M_n = 1.40
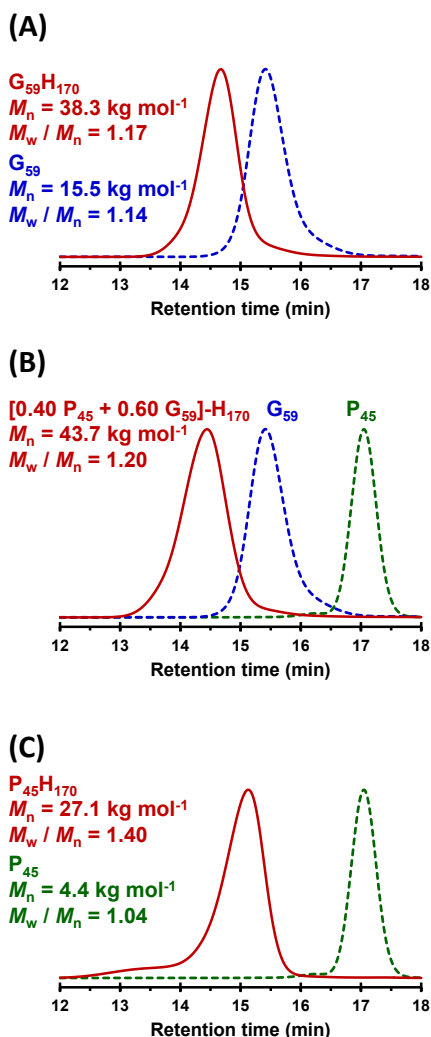P$_{45}$
M_n = 4.4 kg mol^{-1}
M_w / M_n = 1.04

Figure 2. Normalized DMF GPC curves obtained for: (A) the PGMA-PHPMA$_{170}$ diblock copolymer and the corresponding PGMA$_{59}$ precursor; (B) [0.40 PEG$_{45}$ + 0.60 PGMA$_{59}$] - PHPMA$_{170}$ diblock copolymer; (C) the PEG$_{45}$-PHPMA$_{170}$ diblock copolymer and the corresponding PEG$_{45}$ precursor. The blue and green dotted lines shown in (B) indicate the PGMA$_{59}$ and PEG$_{45}$ precursors, respectively. Molecular weight data are expressed relative to poly(methyl methacrylate) calibration standards. [N.B. 'P' denotes PEG, 'G' represents PGMA and 'H' stands for PHPMA].

because the PEG$_{45}$ molecular weight (~2.3 kg mol^{-1}) is significantly lower than that of PGMA$_{59}$ (~9.9 kg mol^{-1}). However, significantly broader (and occasionally multimodal) molecular weight distributions were observed for x = 1.00. PEG$_{45}$ underwent efficient chain extension with HPMA but this precursor alone is not sufficiently long to act as an effective steric stabilizer during PISA syntheses performed at 50 °C. Thus PEG$_{45}$-PHPMA$_n$ diblock copolymers formed insoluble yellow precipitates at intermediate monomer conversions (**Figure S4**). Since unreacted HPMA and free radical initiator remain in the aqueous phase, free radical polymerization of HPMA can occur to produce a white precipitate. This resulted in biphasic

solutions containing yellow and white precipitates with GPC analysis indicating relatively broad MWDs (**Figure 2C**). Poor RAFT control was also encountered for PEG$_{45}$-rich binary compositions such as x = 0.80 when targeting PHPMA DPs of 150 or higher. Recently, PEG$_{45}$ has been reported to act as a steric stabilizer for PISA syntheses performed in either water[46] or alcohol/water mixtures.[57] However, such polymerizations were conducted at 20 °C using photoinitiation, rather than thermal initiation at 50 °C as in the present study. Given the well-known temperature-dependent aqueous solubility of PEG,[58] the reaction temperature is a critical parameter in determining the colloidal stability – and hence success - of such PISA syntheses. In this context, it is perhaps worth emphasizing that good RAFT control (i.e. M_w/M_n < 1.20) was observed for most of the PISA formulations reported in the present study.

Concentrated aqueous dispersions of sterically-stabilized nanoparticles were obtained in all cases where x ≤ 0.80. Each diblock copolymer composition was analyzed by transmission electron microscopy (TEM) to identify the predominant copolymer morphology. This enabled construction of a pseudo-phase diagram (**Figure 3**), which we have previously shown to be essential for reproducibly targeting the otherwise elusive worm morphology.[44, 59, 60]

Route 1: [x PEG$_{45}$ + y PGMA$_{59}$]-PHPMA$_n$
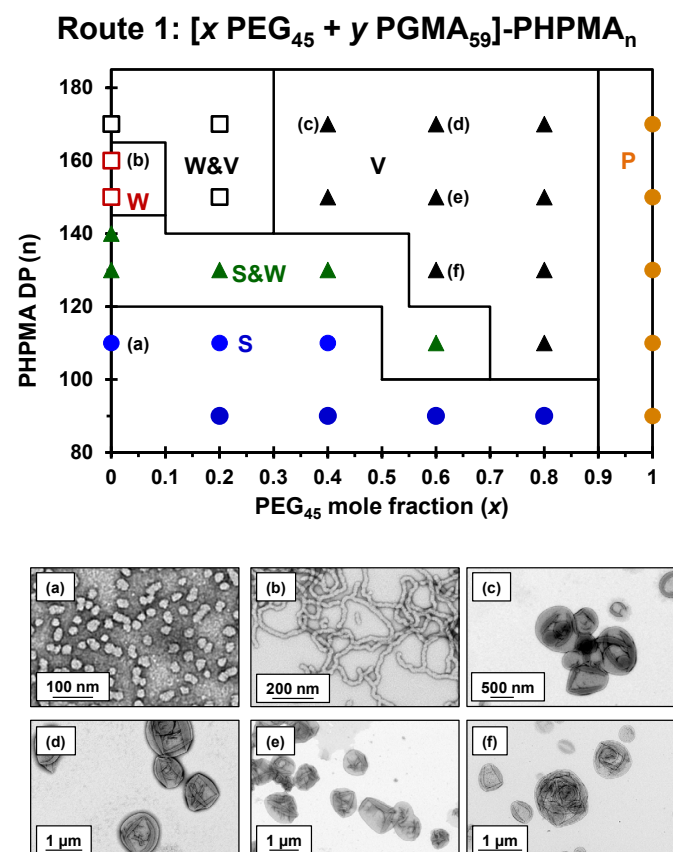
Figure 3. Phase diagram constructed for the RAFT aqueous dispersion polymerization of HPMA at 50 °C using a binary mixture of PEG$_{45}$ and PGMA$_{59}$ precursors to target 10% w/w solids. The diblock copolymer composition is denoted as [x PEG$_{45}$ + y PGMA$_{59}$]-PHPMA$_n$, where x and y are the mole fractions of PEG$_{45}$ and PGMA$_{59}$ respectively and n is the target

PHPMA DP [S = spheres, W = worms, V = vesicles, P = precipitate]. Six representative TEM images are shown for: (a) spheres where x = 0.00, n = 110, (b) worms where x = 0.00, n = 160, (c) vesicles where x = 0.40, n = 170, (d) vesicles where x = 0.60, n = 170, (e) vesicles where x = 0.60, n = 150 and (f) oligolamellar vesicles where x = 0.60, n = 130.

As the relative proportion of the PEG_{45} stabilizer block is increased for any given PHPMA DP, this leads to a progressive evolution from lower order copolymer morphologies (e.g. spheres, worms) towards vesicles, with macroscopic precipitation being observed for the PEG_{45}-rich formulations. Similar observations were reported by Penfold *et al.*[20] when using binary mixtures of PEG_{45} and PEG_{113} stabilizer blocks to target thermoresponsive worms. However, in the present case the only examples of pure worms were obtained in the absence of any PEG_{45} stabilizer, i.e. when targeting $PGMA_{59}$-$PHPMA_{150}$ or $PGMA_{59}$-$PHPMA_{160}$ compositions. Thus, this PISA formulation cannot be used to prepare worm gels with variable hydroxyl functionality, which is the main objective of the current study.

Route 2: Synthesis of [z PEG$_{113}$ + y PGMA$_{59}$]-PHPMA$_n$ diblock copolymer nano-objects.

In view of the experimental observations made when using Route 1, we examined whether a pure worm phase could be accessed by Route 2 (**Scheme 2**). Accordingly, a series of [z PEG$_{113}$ + y PGMA$_{59}$] - PHPMA$_n$ diblock copolymer nano-objects was prepared by adjusting the PEG$_{113}$ and PGMA$_{59}$ mole fractions (z, y) while systematically varying the target PHPMA DP (n) from 140 to 240. Again, all such PISA formulations were conducted at 50 °C for 4 h targeting 10% w/w solids. As expected, targeting higher PHPMA DPs resulting in higher M_n values with relatively narrow molecular weight distributions and high blocking efficiencies, as judged by DMF GPC studies (**see Figure 4**). For each PISA formulation, more than 99% HPMA conversion was determined by ^{1}H NMR spectroscopy (**Table S2**). In addition, this technique was used to confirm the diblock copolymer composition by comparing the integrated proton signals observed for the common methacrylic backbone and pendent PHPMA methyl groups to the oxymethylene proton signals assigned to the PEG chains and the oxyethylene signals assigned to the GMA and HPMA repeat units at 3.5–4.3 ppm. A representative ^{1}H NMR spectrum recorded for [0.40 PEG$_{113}$ + 0.60 PGMA$_{59}$]-PHPMA$_{130}$ redissolved in CD$_3$OD after freeze-drying the as-synthesized aqueous dispersion is given **in Figure 5**.

Initially, a range of [z PEG$_{113}$ + y PGMA$_{59}$]-PHPMA$_n$ diblock copolymers were targeted for z = 0.00 (**Figure 6**). Where the PHPMA DP values overlapped, the PGMA$_{59}$-PHPMA$_n$ copolymer morphologies observed by TEM were in satisfactory agreement with those reported in **Figure 3** for the vertical line represented by x = 0.00. This serves to illustrate the reproducible nature of such aqueous PISA formulations. An important observation for this phase diagram is that, for a fixed PHPMA DP, increasing the mole fraction of the PEG$_{113}$ steric stabilizer always favors the formation of lower order morphologies. For example, when targeting n = 200, pure vesicles can be obtained for the interval $0 \leq z \leq 0.30$, while a mixed phase comprising vesicles and worms

is observed for $0.40 \leq z \leq 0.60$ and pure worms are produced for $0.70 \leq z \leq 1.00$ (see two of the three TEM images shown in **Figure 6** for confirmation of this trend). Similarly, when targeting n = 160, pure worms correspond to the interval $0 \leq z \leq 0.20$, while a worm/sphere mixed phase is observed for $0.30 \leq z \leq 0.80$ and pure spheres are obtained for z = 0.90 and z = 1.00. These observations are rationalized as follows. According to the GPC data shown in **Figure** 4, the PGMA$_{59}$ stabilizer chains (theoretical M_n = 7.5 kg mol^{-1}) occupy a larger hydrodynamic volume than the PEG$_{113}$ chains (theoretical M_n = 5.5 kg mol^{-1}). Thus, as the relative mole fraction of PEG$_{113}$ stabilizer is progressively increased while targeting a fixed PHPMA DP, this necessarily leads to a reduction in the relative volume fraction occupied by the stabilizer block. If the volume occupied by the hydrophobic PHPMA block is constant (because its target DP has been fixed), then this must result in a lower fractional packing parameter, P, which in turn favors the formation of lower order morphologies.[61, 62]
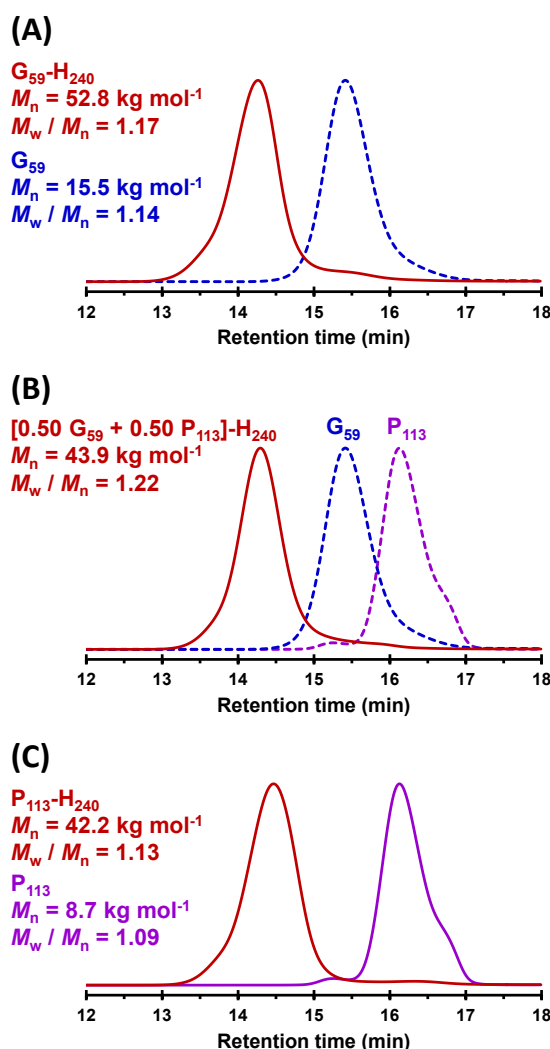

(A)

G_{59}-H_{240}
M_n = 52.8 kg mol^{-1}
M_w / M_n = 1.17
G_{59}
M_n = 15.5 kg mol^{-1}
M_w / M_n = 1.14

(B)

[0.50 G_{59} + 0.50 P_{113}]-H_{240}
M_n = 43.9 kg mol^{-1}
M_w / M_n = 1.22
G_{59} P_{113}

(C)

P_{113}-H_{240}
M_n = 42.2 kg mol^{-1}
M_w / M_n = 1.13
P_{113}
M_n = 8.7 kg mol^{-1}
M_w / M_n = 1.09

Figure 4. DMF GPC curves obtained for: (A) PGMA$_{59}$-PHPMA$_{240}$ diblock copolymer and the corresponding PGMA$_{59}$ precursor; (B) [0.50 PEG$_{45}$ + 0.50 PGMA$_{59}$]-PHPMA$_{240}$ diblock copolymer; (C) PEG$_{113}$-PHPMA$_{240}$ diblock copolymer and the corresponding PEG$_{113}$ precursor. The blue and purple dotted lines shown in (A) and (B) represent the PGMA$_{59}$

and PEG$_{113}$ precursors, respectively. Molecular weight data are expressed relative to poly(methyl methacrylate) calibration standards. [N.B. 'P' denotes PEG, 'G' represents PGMA and 'H' stands for PHPMA].
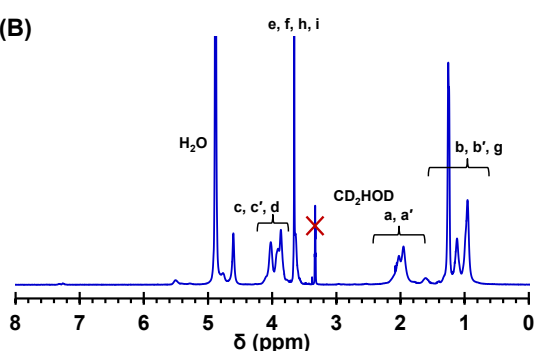
(A) [0.40 PEG$_{113}$ + 0.60 PGMA$_{59}$]-PHPMA$_{130}$
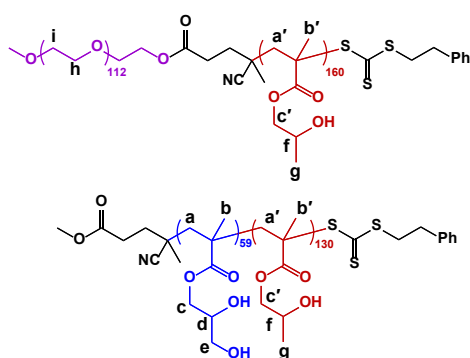
(B)

Figure 5. (A) Chemical structures and (B) ^{1}H NMR spectrum recorded for a [0.40 PEG$_{113}$ + 0.60 PGMA$_{59}$]-PHPMA$_{130}$ diblock copolymer in CD$_3$OD after freeze-drying the as-synthesized aqueous dispersion. The expected diblock copolymer composition was confirmed by comparing the integrated proton signals at 3.5–4.3 ppm to the proton signals at 0.6–2.4 ppm.

It is perhaps worth emphasizing that, compared to other pseudo-phase diagrams for aqueous PISA formulations,[20, 27, 44, 59, 60] the worm phase is unusually broad (see the filled and open red squares shown in **Figure 6**). Each of these twenty pure worm compositions formed soft free-standing gels at ambient temperature owing to multiple inter-worm contacts.[26] One of the main objectives of the present study was to identify diblock copolymer compositions that exhibit *thermoreversible* (de)gelation behavior. This is considered to be essential for cell biology applications, not least because it enables facile sterilization via cold ultrafiltration. Initially, the thermoresponsive behavior of these worm gels was assessed by visual inspection, i.e. tube inversion experiments. Accordingly, 10% w/w aqueous dispersions were cooled to 4 °C by placing in a refrigerator overnight. In all cases, degelation occurred as a result of a worm-to-sphere transition. Each dispersion was then stored at 25 °C for 24 h in an attempt to induce regelation. The nine diblock copolymer compositions for which regelation was observed after this thermal cycle correspond to $z \leq 0.60$ when targeting PHPMA DPs ≤ 180, as indicated by the open red squares shown in **Figure 6**. In contrast, the eleven worm gels obtained for $z \geq 0.70$ when targeting PHPMA DPs ≥ 200

exhibited *irreversible* thermoresponsive behavior, with regelation not occurring at room temperature on normal experimental timescales (see filled red squares in **Figure 6**).
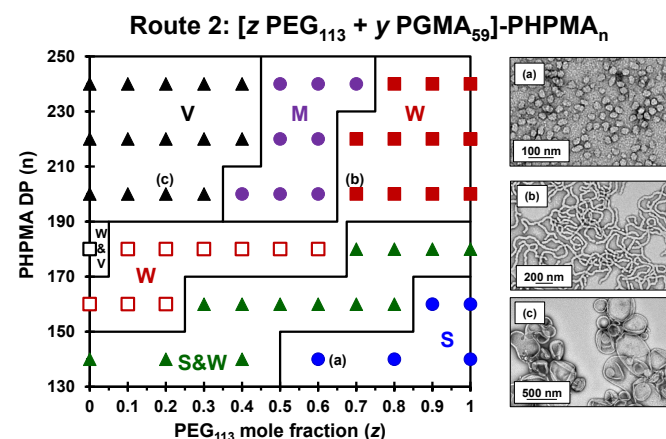
Route 2: [z PEG$_{113}$ + y PGMA$_{59}$]-PHPMA$_n$

Figure 6. Phase diagram constructed for the RAFT aqueous dispersion polymerization of HPMA at 50 °C using a binary mixture of PEG$_{113}$ and PGMA$_{59}$ precursors to target 10% w/w solids. The diblock copolymer composition is denoted as [z PEG$_{113}$ + y PGMA$_{59}$]-PHPMA$_n$, where z and y are the mole fractions of PEG$_{113}$ and PGMA$_{59}$ respectively and n is the target PHPMA DP [S = spheres, W = worms, M = mixed phase, V = vesicles, P = precipitate]. Three representative TEM images are shown for: (a) spheres where z = 0.60 and n = 140, (b) worms where z = 0.70 and n = 200 and (c) vesicles where x = 0.20 and n = 200.

This is understandable because such compositions are both PEG$_{113}$-rich and also comprise relatively long PHPMA blocks, with both parameters known to favor either irreversible or zero thermoresponsive behavior, respectively.[44, 63] Following these qualitative experiments, three worm gels were selected for further temperature-dependent oscillatory rheology studies. These three worm gels had an identical PHPMA DP (n = 160) and a PEG$_{113}$ mole fraction z of 0.00, 0.10 or 0.20 (**Figure 7**). When studying the rheological behavior of similar PGMA$_{54}$-PHPMA$_y$ diblock copolymer worm gels, Verber *et al.* initially reported irreproducible G' data which was attributed to differing thermal and/shear histories.[6] Fortunately, this problem was eliminated simply by conducting a cooling-heating cycle to 'reset' each gel via a worm-to-sphere transition. The same approach was adopted in the present study for the three gels shown in **Figure 7**. Accordingly, each 10% w/w aqueous worm dispersion was first cooled to 4 °C for 60 min followed by incubation at 25 °C for 24 h prior to oscillatory rheological measurements. Then, the storage modulus G' (filled circles) and the loss modulus G'' (open circles) were determined from 25 °C to 4 °C to 25 °C at a constant strain of 1.0% and an angular frequency of 1.0 rad s^{-1}, with 5 min being allowed for thermal equilibration at each temperature (**Figure 7**). Blue and red data sets represent the cooling and heating stages respectively while representative TEM images obtained for each type of diblock copolymer worm dispersion are also shown.

The z = 0.00 worm gel exhibits an initial G' of 73 Pa at 25 °C, which is reduced by two orders of magnitude for the corresponding free-flowing dispersion of spheres that is produced on cooling to 4 °C (**Figure 7A**). In addition, the point

of intersection (or cross-over) of the G' and G'' curves indicates a critical gelation temperature (CGT) of 12 °C.
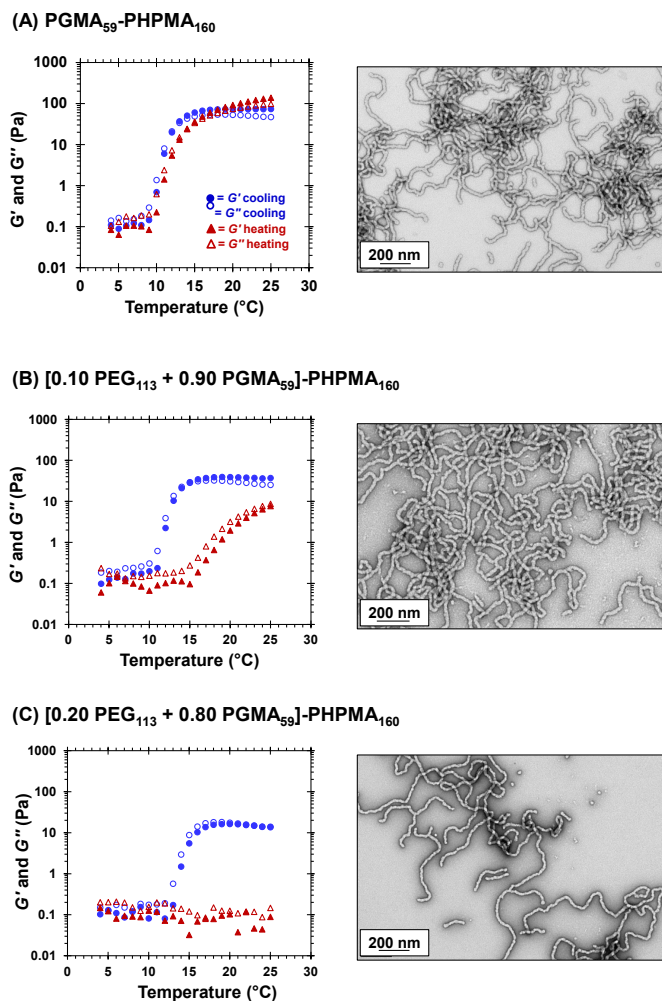
(A) PGMA$_{59}$-PHPMA$_{160}$

(B) [0.10 PEG$_{113}$ + 0.90 PGMA$_{59}$]-PHPMA$_{160}$

(C) [0.20 PEG$_{113}$ + 0.80 PGMA$_{59}$]-PHPMA$_{160}$

Figure 7. Temperature-dependent oscillatory rheology studies of a series of [z PEG$_{113}$ + y PGMA$_{59}$]-PHPMA$_{160}$ diblock copolymer worm gels: (A) z = 0.00, (B) z = 0.10 and (C) z = 0.20. These measurements were conducted on 10% w/w aqueous dispersions at a fixed strain of 1.0% and an angular frequency of 1.0 rad s^{-1}, allowing a thermal equilibration time of 5 min at each temperature. All gels were cooled to 4 °C for 1 h and then warmed up to 25 °C for 24 h to reset the gel prior to analysis in order to remove any thermal history. The filled and open symbols represent the storage modulus (G') and the loss modulus (G''), respectively. The blue circles and red triangles represent the cooling and heating cycles, respectively. Representative TEM images recorded after drying dilute dispersions of the as-synthesized diblock copolymer worms at 25 °C are shown in each case.

Minimal hysteresis was observed on returning to 25 °C, although a somewhat higher G' of 138 Pa was obtained. This (de)gelation behavior is more or less consistent with that reported by Verber *et al.* for a closely-related PGMA$_{54}$-PHPMA$_{160}$ diblock copolymer.[6] However, incorporating just 10 mol% PEG$_{113}$ (z = 0.10) as a co-stabilizer block has a substantial effect on both the worm gel strength and the thermoresponsive behavior (**Figure 7B**). The initial G' is halved to 36 Pa at 25 °C, which unfortunately indicates that there is no significant hydrogen bonding interactions between the PGMA chains on any given worm with PEG chains on neighbouring worms.

Moreover, the CGT for this second diblock copolymer worm gel is slightly higher at 15 °C. Furthermore, the heating curve observed for this sample (**Figure 7B**, red circles) reveals that full regelation (G' = 9 Pa) does not occur on the timescale of this experiment. This relatively slow response is not ideal for cell biology applications. The negative influence of the PEG$_{113}$ co-stabilizer is even more pronounced at z = 0.20 (**Figure 7C**). In this case, the worm gel exhibits an initial G' of 13 Pa at 25 °C and its CGT is 23 °C. Inspection of the heating curve (**Figure 7C**, red circles) indicates that the sphere-to-worm transition required for regelation does not occur on the timescale of this rheology experiment. Clearly, the addition of either 10 or 20 mol% PEG$_{113}$ stabilizer to the PEG$_{113}$-PHPMA$_{220}$ worms significantly retards the kinetics of sphere-to-worm transition, as observed in Figure 7. It is perhaps worth emphasizing that this particular worm gel had already been successfully 'reset' prior to these rheology experiments, which indicates that regelation can occur at 25 °C within 24 h. Unfortunately, this timescale is far too long for cell biology applications.

Conclusions

The feasibility of using a binary mixture of a hydroxylated (PGMA$_{59}$) and a non-hydroxylated (PEG$_{45}$ or PEG$_{113}$) steric stabilizer block for the synthesis of thermoresponsive diblock copolymer worm gels via aqueous PISA has been explored. This approach was explored with the aim of identifying new compositions that would exhibit thermoreversible (de)gelation behavior for potential cell biology applications. Prior concerns regarding the possibility of the formation of insoluble hydrogen-bonded complexes proved to be groundless: the PGMA and PEG steric stabilizers proved to be mutually compatible in all proportions. However, the PGMA$_{59}$/PEG$_{45}$ formulation proved to be rather fruitless, with no examples of pure worm gels being identified when constructing a pseudo-phase diagram. In contrast, the PGMA$_{59}$/PEG$_{113}$ formulation yielded twenty diblock copolymer compositions that produced a pure worm morphology as judged by TEM studies. Unfortunately, eleven of these examples exhibited irreversible thermoresponsive behavior: the degelation that occurred on cooling owing to a worm-to-sphere transition was not followed by regelation on returning to ambient temperature. Moreover, examining three of the remaining nine examples revealed that incorporating just 10-20 mol% PEG$_{113}$ had a detrimental effect on the worm gel modulus and also substantially extended the timescale required for regelation. Nevertheless, this study suggests that hybrid PGMA/PEG worm gels exhibiting thermoreversible (de)gelation behavior may be accessible. This would most likely require using a PEG$_n$ block exhibiting an *intermediate* mean degree of polymerization (n = 55-70). If such an approach proved to be successful, it would enable the rational design of a library of worm gels of similar softness (i.e. comparable bulk moduli) but with variable hydroxyl content. In principle, this should enable the *minimum hydroxyl content* required to induce stasis in embryonic human stem cells to be determined.

ARTICLE   Journal Name

Conflicts of interest

There are no conflicts to declare.

Acknowledgements

Notes and references

1.   A. K. Bajpai, S. K. Shukla, S. Bhanu and S. Kankane, *Progress in Polymer Science*, 2008, **33**, 1088-1118.
2.   N. Rapoport, *Progress in Polymer Science*, 2007, **32**, 962-990.
3.   D. Schmaljohann, *Advanced Drug Delivery Reviews*, 2006, **58**, 1655-1670.
4.   C. d. l. H. Alarcon, S. Pennadam and C. Alexander, *Chemical Society Reviews*, 2005, **34**, 276-285.
5.   A. S. Hoffman, *Advanced Drug Delivery Reviews.*, 2002, **54**, 3-12.
6.   G. Chen and A. S. Hoffman, *Nature*, 1995, **373**, 49-52.
7.   P. S. Stayton, T. Shimoboji, C. Long, A. Chilkoti, G. Chen, J. M. Harris and A. S. Hoffman, *Nature*, 1995, **378**, 472-474.
8.   R. Zhang, H. K. Mjoseng, M. A. Hoeve, N. G. Bauer, S. Pells, R. Besseling, S. Velugotla, G. Tourniaire, R. E. B. Kishen, Y. Tsenkina, C. Armit, C. R. E. Duffy, M. Helfen, F. Edenhofer, P. A. de Sousa and M. Bradley, *Nature Communications*, 2013, **4**, 1335.
9.   B. V. Slaughter, S. S. Khurshid, O. Z. Fisher, A. Khademhosseini and N. A. Peppas, *Advanced Materials*, 2009, **21**, 3307-3329.
10.   N. A. Peppas, J. Z. Hilt, A. Khademhosseini and R. Langer, *Advanced Materials*, 2006, **18**, 1345-1360.
11.   J. R. Spence, C. N. Mayhew, S. A. Rankin, M. F. Kuhar, J. E. Vallance, K. Tolle, E. E. Hoskins, V. V. Kalinichenko, S. I. Wells, A. M. Zorn, N. F. Shroyer and J. M. Wells, *Nature*, 2011, **470**, 105-109.
12.   M. A. Lancaster and J. A. Knoblich, *Nature Protocols*, 2014, **9**, 2329-2340.
13.   R. Cruz-Acuna, M. Quiros, A. E. Farkas, P. H. Dedhia, S. Huang, D. Siuda, V. Garcia-Hernandez, A. J. Miller, J. R. Spence, A. Nusrat and A. J. Garcia, *Nature Cell Biology*, 2017, **19**, 1326-1335.
14.   A. S. Hoffman, *Advanced Drug Delivery Reviews*, 2013, **65**, 10-16.
15.   J. F. Mano, *Advanced Engineering Materials*, 2008, **10**, 515-527.
16.   N. Corrigan, J. Yeow, P. Judzewitsch, J. Xu and C. Boyer, *Angewandte Chemie International Edition*, 2019, **58**, 5170-5189.
17.   Q. Tian, C. Fei, H. Yin and Y. Feng, *Progress in Polymer Science*, 2019, **89**, 108-132.
18.   Y. Pei, A. B. Lowe and P. J. Roth, *Macromolecular Rapid Communications*, 2017, **38**, 1600528.
19.   Q. Ye, M. Huo, M. Zeng, L. Liu, L. Peng, X. Wang and J. Yuan, *Macromolecules*, 2018, **51**, 3308-3314.
20.   N. J. W. Penfold, J. R. Whatley and S. P. Armes, *Macromolecules*, 2019, **52**, 1653-1662.
21.   N. J. W. Penfold, J. Yeow, C. Boyer and S. P. Armes, *Acs Macro Lett*, 2019, **8**, 1029-1054.
22.   Z. Chu, C. A. Dreiss and Y. Feng, *Chemical Society Reviews*, 2013, **42**, 7174-7203.
23.   J. Rieger, *Macromolecular Rapid Communications*, 2015, **36**, 1458-1471.
24.   A. Blanazs, R. Verber, O. O. Mykhaylyk, A. J. Ryan, J. Z. Heath, C. W. Douglas and S. P. Armes, *Journal of the American Chemical Society*, 2012, **134**, 9741-9748.
25.   R. Verber, A. Blanazs and S. P. Armes, *Soft Matter*, 2012, **8**, 9915-9922.
26.   J. R. Lovett, M. J. Derry, P. Yang, F. L. Hatton, N. J. Warren, P. W. Fowler and S. P. Armes, *Chemical Science*, 2018, **9**, 7138-7144.
27.   M. Sponchioni, C. T. O'Brien, C. Borchers, E. Wang, M. N. Rivolta, N. J. W. Penfold, I. Canton and S. P. Armes, *Chemical Science*, 2020, **11**, 232-240.
28.   R. Spelat, F. Ferro, P. Contessotto, N. J. Warren, G. Marsico, S. P. Armes and A. Pandit, *Materials Today Bio*, 2020, **5**, 100040.
29.   K. A. Simon, N. J. Warren, B. Mosadegh, M. R. Mohammady, G. M. Whitesides and S. P. Armes, *Biomacromolecules*, 2015, **16**, 3952-3958.
30.   M. B. Renfree and G. Shaw, *International Journal of Development Biology*, 2014, **58**, 175-181.
31.   M. K. Kocik, O. O. Mykhaylyk and S. P. Armes, *Soft Matter*, 2014, **10**, 3984-3992.
32.   N. J. W. Penfold, J. R. Lovett, P. Verstraete, J. Smets and S. P. Armes, *Polymer Chemistry*, 2017, **8**, 272-282.
33.   V. J. Cunningham, L. P. D. Ratcliffe, A. Blanazs, N. J. Warren, A. J. Smith, O. O. Mykhaylyk and S. P. Armes, *Polymer Chemistry*, 2014, **5**, 6307-6317.
34.   I. Canton, N. J. Warren, A. Chahal, K. Amps, A. Wood, R. Weightman, E. Wang, H. Moore and S. P. Armes, *ACS central science*, 2016, **2**, 65-74.
35.   J. M. Harris and R. B. Chess, *Nature Reviews Drug Discovery*, 2003, **2**, 214-221.
36.   F. M. Veronese and G. Pasut, *Drug Discovery Today*, 2005, **10**, 1451-1458.
37.   P. Milla, F. Dosio and L. Cattel, *Current Drug Metabolism*, 2012, **13**, 105-119.
38.   J. He, Q. Xu, J. Tan, L. Zhang, J. Tan and L. Zhang, *Macromolecular Rapid Communications*, 2019, **40**, e1800296.
39.   Y. X. Zhang, L. L. Yu, X. C. Dai, L. Zhang and J. B. Tan, *Acs Macro Lett*, 2019, **8**, 1102-1109.
40.   Y. J. Ma, P. Gao, Y. Ding, L. L. Huang, L. Wang, X. H. Lu and Y. L. Cai, *Macromolecules*, 2019, **52**, 1033-1041.
41.   J.-T. Sun, C.-Y. Hong and C.-Y. Pan, *Polymer Chemistry*, 2013, **4**, 873-881.
42.   F. D'Agosto, J. Rieger and M. Lansalot, *Angewandte Chemie International Edition*, 2020, **59**, 8368-8392.
43.   J. Rieger, C. Grazon, B. Charleux, D. Alaimo and C. Jerome, *Journal of Polymer Science Part A: Polymer Chemistry*, 2009, **47**, 2373-2390.
44.   N. J. Warren and S. P. Armes, *Journal of the American Chemical Society*, 2014, **136**, 10174-10185.

45. L. D. Blackman, K. E. B. Doncom, M. I. Gibson and R. K. O'Reilly, *Polymer Chemistry*, 2017, **8**, 2860-2871.
46. K. Ren and J. Perez-Mercader, *Polymer Chemistry*, 2017, **8**, 3548-3552.
47. N. J. W. Penfold, Y. Ning, P. Verstraete, J. Smets and S. P. Armes, *Chemical Science*, 2016, **7**, 6894-6904.
48. M. Semsarilar, V. Ladmiral, A. Blanazs and S. P. Armes, *Langmuir* 2012, **28**, 914-922.
49. V. Ladmiral, M. Semsarilar, I. Canton and S. P. Armes, *Journal of the American Chemical Society*, 2013, **135**, 13574-13581.
50. C. Gonzato, M. Semsarilar, E. R. Jones, F. Li, G. J. P. Krooshof, P. Wyman, O. O. Mykhaylyk, R. Tuinier and S. P. Armes, *Journal of the American Chemical Society*, 2014, **136**, 11100-11106.
51. M. Williams, N. J. W. Penfold and S. P. Armes, *Polymer Chemistry*, 2016, **7**, 384-393.
52. M. Williams, N. J. W. Penfold, J. R. Lovett, N. J. Warren, C. W. I. Douglas, N. Doroshenko, P. Verstraete, J. Smets and S. P. Armes, *Polymer Chemistry*, 2016, **7**, 3864-3873.
53. M. J. Rymaruk, K. L. Thompson, M. J. Derry, N. J. Warren, L. P. D. Ratcliffe, C. N. Williams, S. L. Brown and S. P. Armes, *Nanoscale*, 2016, **8**, 14497-14506.
54. M. Semsarilar, E. R. Jones, A. Blanazs and S. P. Armes, *Advanced Materials*, 2012, **24**, 3378-3382.
55. N. J. W. Penfold, J. R. Lovett, N. J. Warren, P. Verstraete, J. Smets and S. P. Armes, *Polymer Chemistry*, 2016, **7**, 79-88.
56. E. R. Jones, M. Semsarilar, A. Blanazs and S. P. Armes, *Macromolecules*, 2012, **45**, 5091-5098.
57. J. Tan, X. Li, R. Zeng, D. Liu, Q. Xu, J. He, Y. Zhang, X. Dai, L. Yu, Z. Zeng and L. Zhang, *Acs Macro Lett*, 2018, **7**, 255-262.
58. F. E. Bailey, Jr. and R. W. Callard, *Journal of Applied Polymer Science*, 1959, **1**, 56-62.
59. S. Sugihara, A. Blanazs, S. P. Armes, A. J. Ryan and A. L. Lewis, *Journal of the American Chemical Society*, 2011, **133**, 15707-15713.
60. A. Blanazs, A. J. Ryan and S. P. Armes, *Macromolecules*, 2012, **45**, 5099-5107.
61. A. Blanazs, S. P. Armes and A. J. Ryan, *Macromolecular Rapid Communications*, 2009, **30**, 267-277.
62. J. N. Israelachvili, D. J. Mitchell and B. W. Ninham, *Journal of the Chemical Society, Faraday Transactions 2*, 1976, **72**, 1525-1568.
63. N. J. Warren, M. J. Derry, O. O. Mykhaylyk, J. R. Lovett, L. P. D. Ratcliffe, V. Ladmiral, A. Blanazs, L. A. Fielding and S. P. Armes, *Macromolecules*, 2018, **51**, 8357-8371.